

# Elucidation of the atherosclerotic disease process in apo E and wild type mice by vibrational spectroscopy

Fran Adar<sup>\*a</sup>, Linda Jelicks<sup>b</sup>, Coralie Naudin<sup>a</sup>, Denis Rousseau<sup>b</sup>, Syun-ru Yeh<sup>b</sup>  
<sup>a</sup> Jobin Yvon, Inc., 3880 Park Ave., Edison, NJ 08820

<sup>b</sup> Department of Physiology and Biophysics, Albert Einstein School of Medicine,  
Jack and Pearl Resnick Campus Ullmann Building, Rm. 313, 1300 Morris Park  
Ave., Bronx, NY 10461

## Abstract

Raman and FTIR microprobe spectroscopy have been used to characterize the atherosclerotic process in Apo E and wild type mice. The Apo E null mouse is being studied in parallel with a healthy strain as a model of the human atherosclerotic disease. Preliminary Raman microprobe spectra have been recorded from the lumen of the aorta vessels from a normal black mouse (C57BL/6J) and the apo E null mouse fed on a normal chow diet. Spectra were also recorded from another normal mouse fed breeder chow containing a much higher content of fats. In the Raman spectra the fat cells exhibited spectra typical of esterified triglycerides while the wall tissue had spectra dominated by Amide I and III modes and the phenylalanine stretch at  $1003\text{ cm}^{-1}$  of protein. The FTIR spectra showed the typical Amide I and II bands of protein and the strong  $>\text{C}=\text{O}$  stretch of the triglycerides. In addition, there were morphologically distinct regions of the specimens indicating a surprising form of calcification in one very old mouse (wild type), and free fatty acid inclusions in the knock out mouse. The observation of these chemistries provide new information for elucidation of the molecular mechanisms of the development of atherosclerosis.

## 1. Background

Atherosclerosis, a disease causing hardening of blood vessel walls, involves the deposition of lipid, cholesterol, calcium and other components on the inner lining of the vessels. Atherosclerotic plaques, which can contain lipid cores, fibrous caps, and calcification, can cause vessel lumen narrowing (reducing blood flow) or can rupture leading to thrombosis (possibly resulting in heart attack or stroke). Plaque composition may be a more critical determinant of the risk of rupture than lumen size. Non-invasive methods, able to determine plaque composition have the potential to identify vulnerable plaques, susceptible to rupture.

While a number of techniques have been used for studying atherosclerotic vessels<sup>1,2,3</sup> vibrational spectroscopy has been attracting interest because it provides detailed molecular information non-destructively, and possibly in-situ, in the case of Raman spectroscopy<sup>4</sup>. Recent studies have demonstrated the potential of Raman measurements to evaluate atherosclerotic plaque in mice<sup>5,6</sup>. APOE\*3 Leiden transgenic mice carry a dysfunctional apo E variant derived from human patients with a dominantly inherited form of familial dysbetalipoproteinemia. Consequently they exhibit hyperlipidemia resulting in rapid development of atherosclerotic plaque when fed a high fat, high cholesterol diet.

Mice are typically resistant to atherosclerosis<sup>7</sup> but Atherosclerosis can be induced by diet in mice providing an excellent small animal model of human disease. The apo E null mouse<sup>8</sup> is a strain that predictably develops atherosclerotic lesions<sup>9</sup>. Apolipoprotein E, which is involved in the transport of cholesterol and triglycerides, is altered or deleted in the knock-out mouse, and the

---

\* fran.adar@jobinyvon.com; phone 1 732-494-8660; fax 1 732-549-2571; jobinyvon.com

animals develop lesions that are well characterized and similar to those found in humans. The object of the study is to exploit vibrational microspectroscopy to try to correlate histopathological features in the mouse aortas to the chemical composition of the normal mouse as compared to the knockout.

## 2. Experimental Description

Three mice were examined: an aged (ca 15 months) in-bred black mouse (C57BL/6J), an aged (ca 12 months) apo E null mouse (that is, a mouse from a strain developed to be lacking in apolipoprotein E activity), and a younger (12 month) black mouse. The first two mice were fed a normal chow diet (PicoLab® Rodent Diet 20 with normal fat levels) while the third was fed a breeder chow diet (PicoLab® Mouse Diet 20 with moderately high fat). The C57BL/6J strain is inbred and has been used as a control for gene knockouts. They develop obesity when fed a high fat "Western" style diet.

The fat composition of the two diets is shown in Table I. The biggest differences are in the total fat composition (Breeder Chow about twice the fat content of Normal Chow), cholesterol (Breeder Chow 50% higher than Normal Chow), total saturated fatty acids (Breeder Chow almost 4 times higher than Normal Chow) and total monounsaturated fatty acids (Breeder Chow 3 times higher than Normal Chow).

Table I. Fat Composition for Normal and Breeder Chows

|                                   | Normal Chow | Breeder Chow | Ratio |
|-----------------------------------|-------------|--------------|-------|
| Fat Content (ether extract)       | 4.5         | 9.0          | 2.00  |
| Fat Content (acid hydrolysis)     | 5.4         | 9.5          | 1.76  |
| Cholesterol (ppm)                 | 149         | 221          | 1.48  |
| Linoleic Acid                     | 2.26        | 2.34         | 1.04  |
| Linolenic Acid                    | 0.20        | 0.26         | 1.3   |
| Arachidonic Acid                  | <0.01       | 0.01         | -     |
| Omega-3 Fatty Acids               | 0.36        | 0.45         | 1.25  |
| Total Saturated Fatty Acids       | 0.84        | 3.18         | 3.79  |
| Total Monounsaturated Fatty Acids | 1.04        | 3.01         | 2.98  |

Both Raman and FTIR spectra were recorded on the LabRAM-IR. The SensIR™ FTIR interferometer scans the spectrum between 650 and 4000  $\text{cm}^{-1}$ . The LabRAM was used with both the HeNe (633nm) and diode (785nm) lasers with 1800 and 600 g/mm gratings respectively; the dispersion in each case was approximately 1  $\text{cm}^{-1}$ /pixel. Spatial resolution for FTIR is about 20 $\mu\text{m}$ , while the laser spot size for Raman is no greater than 1 $\mu\text{m}$ . The samples were first visualized on the microscope with a TV camera, the spot of interest was chosen, and then the spectrum was recorded. It was found that sometimes the spectrum generated was not what was suspected from the histological characteristics of the spot. So confocal Raman spectra were acquired as a function of depth and a confocal Raman map was created in order to monitor the chemical variations.

## 3. Results and Discussion

The first figure shows the FTIR spectra of a protein-rich and lipid regions. These spectra were recorded with the ATR objective which means that the spectra represent material that is in contact with the objective. It was found much easier to observe the spectrum of lipid than of protein. In this case, this may mean that the spectra represent cell walls which will of course contain a lot of lipid. However, the top spectrum shows the Amide I and II bands, as well as the NH band, of proteinaceous material.

Figure 2 shows typical Raman spectra of proteins and lipids from the lumen side of the aorta of the wild-type mouse fed the normal fat diet. There are several means of distinguishing the two components.

The lipid spectrum has a fairly strong band near  $1650\text{ cm}^{-1}$  due to the double bond in unsaturated fatty acids, and a carbonyl band near  $1750\text{ cm}^{-1}$  when the fatty acids are esterified. There is an intense, broad band near  $1430\text{ cm}^{-1}$  assigned to  $>\text{CH}_2$  deformation, but this band is not useful in differentiation from protein because it is present in protein as well. The lipids also have a characteristic doublet at  $1303$  and  $1264\text{ cm}^{-1}$ .

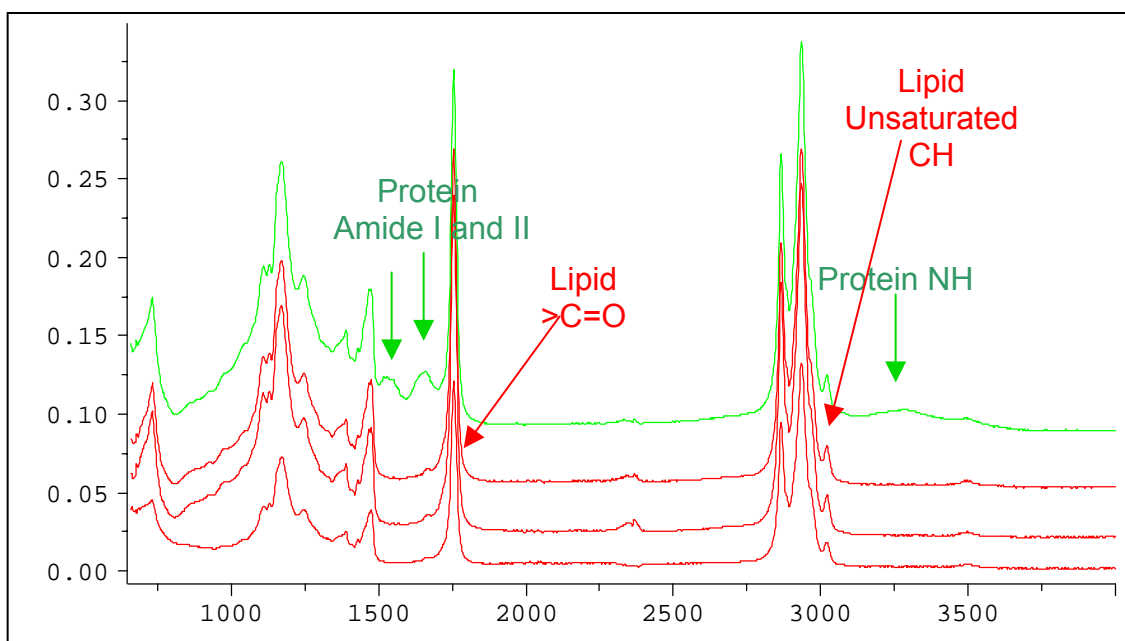


Figure 1. ATR FTIR spectra recorded from a Wild type mouse fed a High fat Diet

The protein spectrum is easily recognized by the broad band which peaks somewhere between  $1640$  and  $1670\text{ cm}^{-1}$  and has been assigned to the Amide I. Unlike the IR spectrum, the Amide II does not appear in the Raman spectrum unless exciting in the UV. There is also a sharp feature at  $1000\text{ cm}^{-1}$  which indicates the presence of phenylalanine.

Figure 3 shows Raman spectra generated from the Apo E knock-out mouse in regions of fat cells (top), protein (bottom), and droplets (middle). The spectrum of the droplets is the most interesting since it lacks much intensity in the carbonyl band at about  $1750\text{ cm}^{-1}$ . This means that **the fatty acids are non-esterified**, an observation which has not been previously noted.

Figure 4 shows spectra recorded from fatty material (upper three spectra) from the region shown in the optical micrograph. The top spectrum is typical of the fat cells whereas the two spectra under that, recorded from dark material, show a very intense band at  $1086$ - $1088\text{ cm}^{-1}$  as well as several other features that coincide with bands of calcite ( $\text{CaCO}_3$ ) which is reproduced in the second spectrum from the bottom. In addition, the spectrum of tooth enamel, an almost pure carbonated hydroxyapatite mineral, is shown on the bottom of the figure. Clearly the **calcification seen in this aorta lumen is calcite not, phosphate**. This is probably the first time that this mineral has been observed in calcified soft tissue.

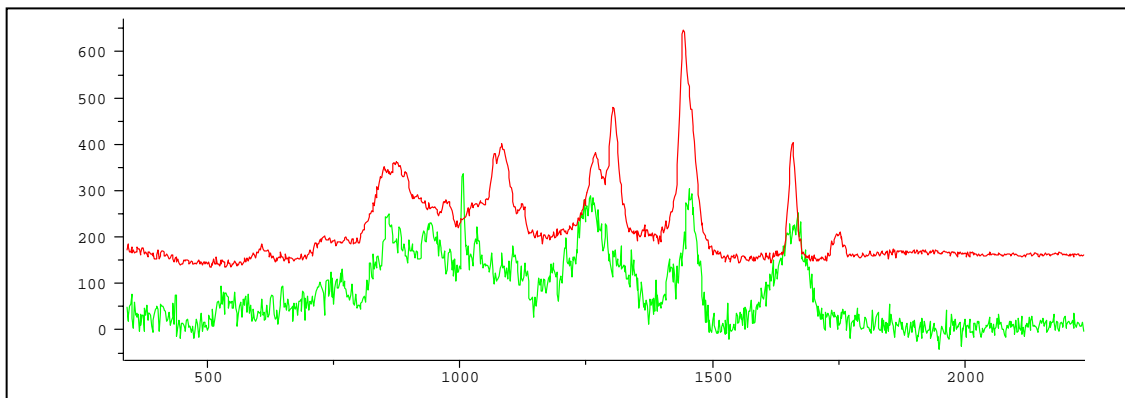


Figure 2. Lipid (top) and protein (bottom) Raman spectra in the fingerprint region of the wild-type mouse fed the normal fat diet

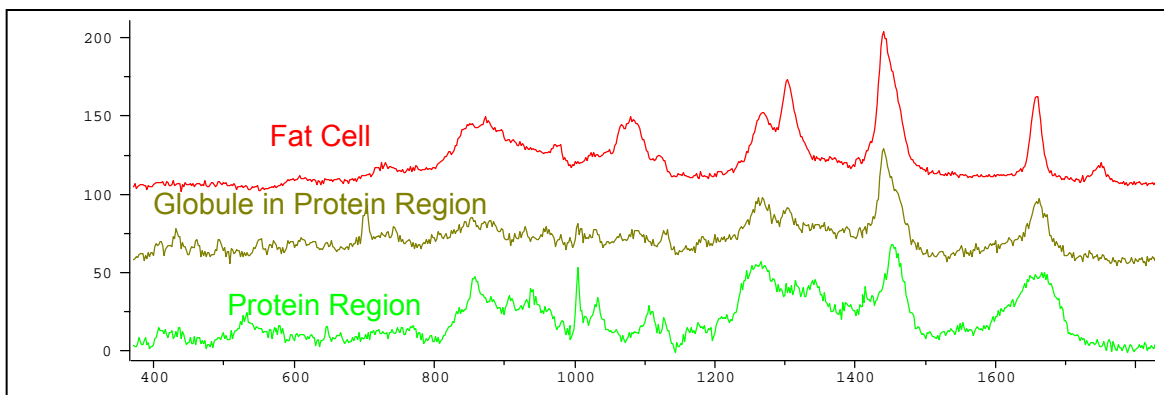


Figure 3. Confocal Raman spectra of Apo E Mouse recorded from Fat Cell, protein Region, and Globule in Protein Region

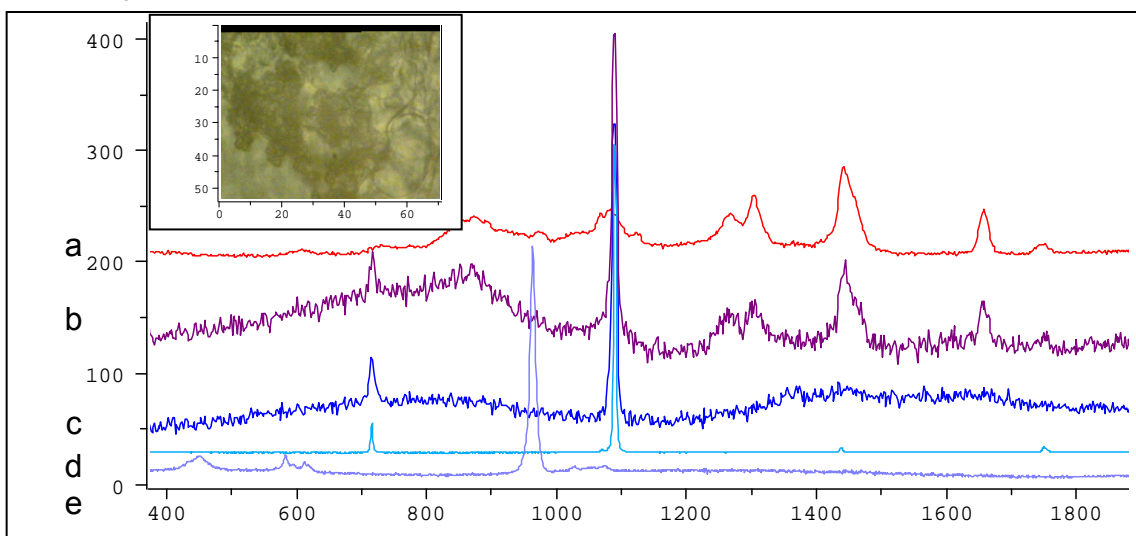


Figure 4. Confocal Raman spectrum of fatty tissue (a), calcified fat tissue (b and c), calcite (d), and tooth enamel or carbonated hydroxyapatite (e).

Sometimes when we attempted to select a region of fat or protein, the spectrum would not be as expected. A crude confocal depth profile indicated that both materials were present, but at different heights. Figure 5 shows the spectra recorded in what appeared to be a fatty region, but at different levels with respect to the top focus. The top spectrum is clearly that of protein; at  $8\mu\text{m}$  below the surface the spectrum of lipid is recorded, while the spectrum in between is a mixture of the two.

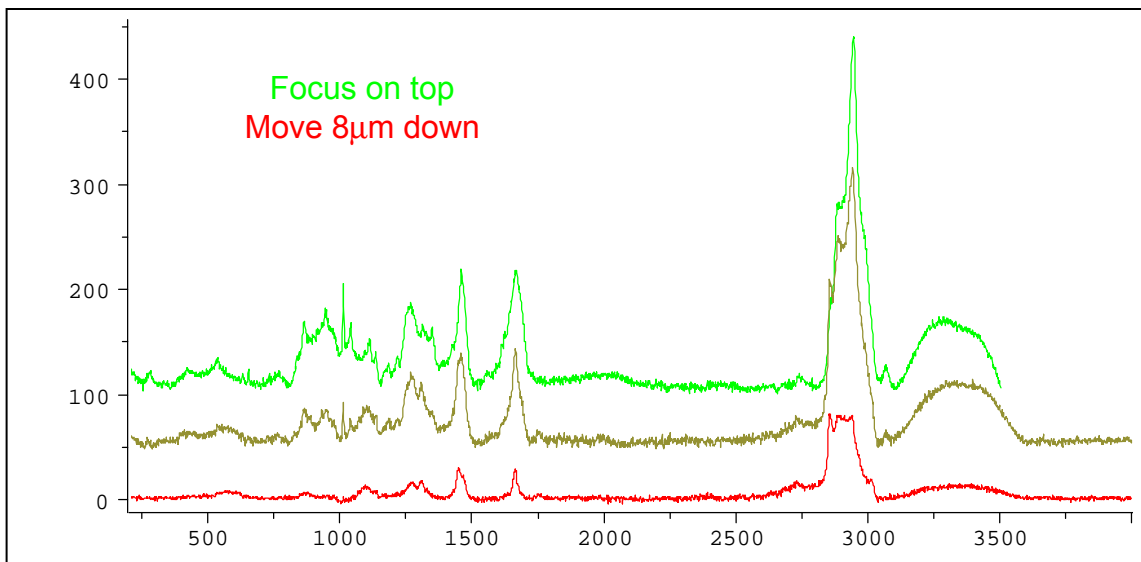


Figure 5. Crude depth profile recorded in fatty region showing the transition from protein to fat as the instrument focus was scanned deeper into the sample.

The next figures show the results of a mapping experiment. The map was performed on the aorta removed from the normal mouse fed on a Breeder Chow™, high fat diet. Figure 6 a and b show the micrograph versus and Raman map of protein and lipid. While mapping is sometimes done by selecting a spectral line characteristic of a species, creating good maps using this method is often not feasible because of overlapping spectral features. Because of this the maps that are presented here were created by “modeling”. In this simple algorithm, each spectrum in the multifile is reconstructed as a superposition of the model spectra. The model spectra were extracted as the purest spectra from the multifile and are reproduced in Figure 7.

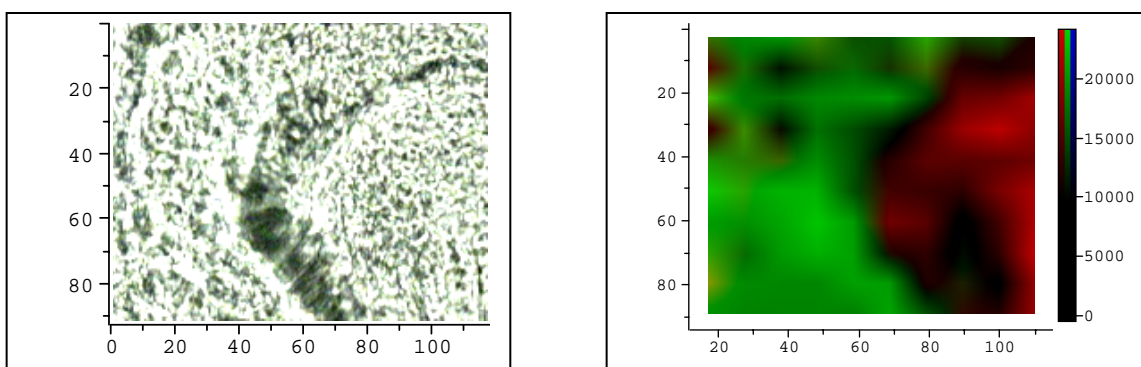


Figure 6a. Micrograph of lumen side of aorta showing fatty and proteinaceous regions. 6b. Raman map of same region, color-coded with green as protein and red as lipid.

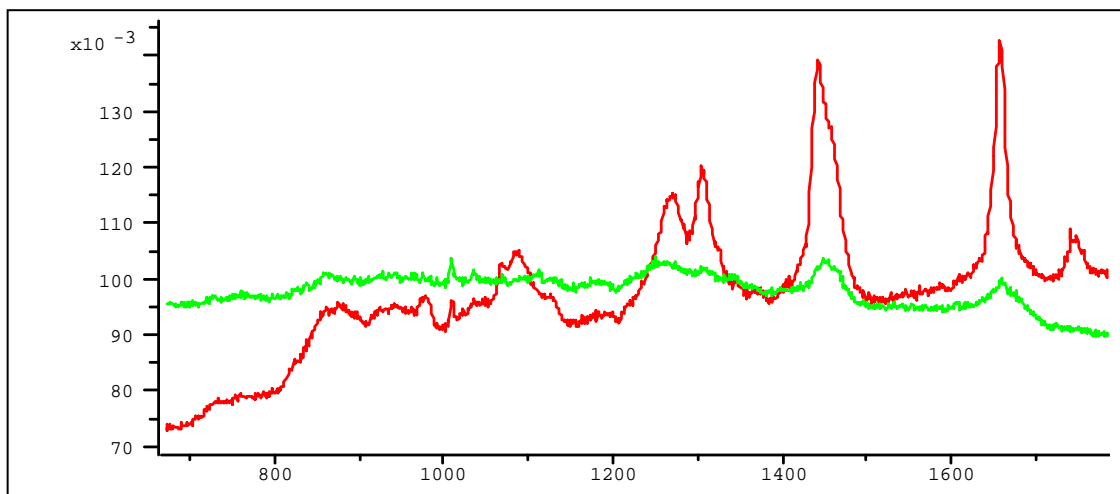


Figure 7. Model Raman spectra for confocal Raman map.

Figure 8 shows the result of the modeling software. A point at the interface between the fat and protein regions was selected with the cursor in the map and the results of the fitting are then reported as a percent of lipid, percent of protein, and error. Figure 9 shows a similar calculation from the lipid droplet.

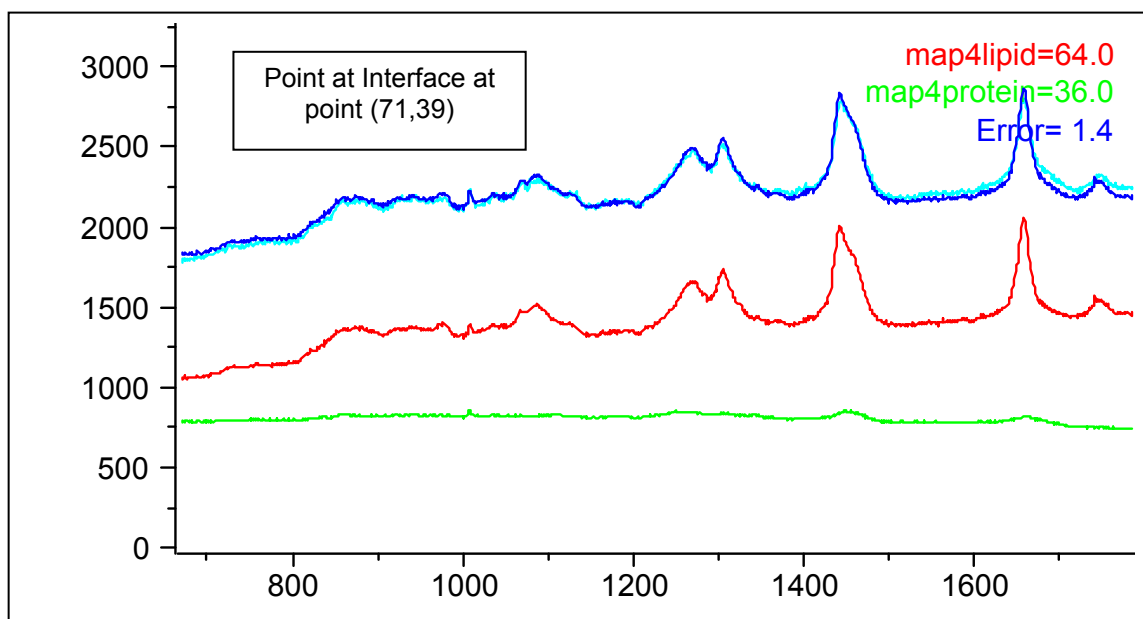


Figure 8. Modelling of spectrum from point at the protein-fat interface showing % lipid, % protein, simulated spectrum overlaid on measured spectrum, and % error.

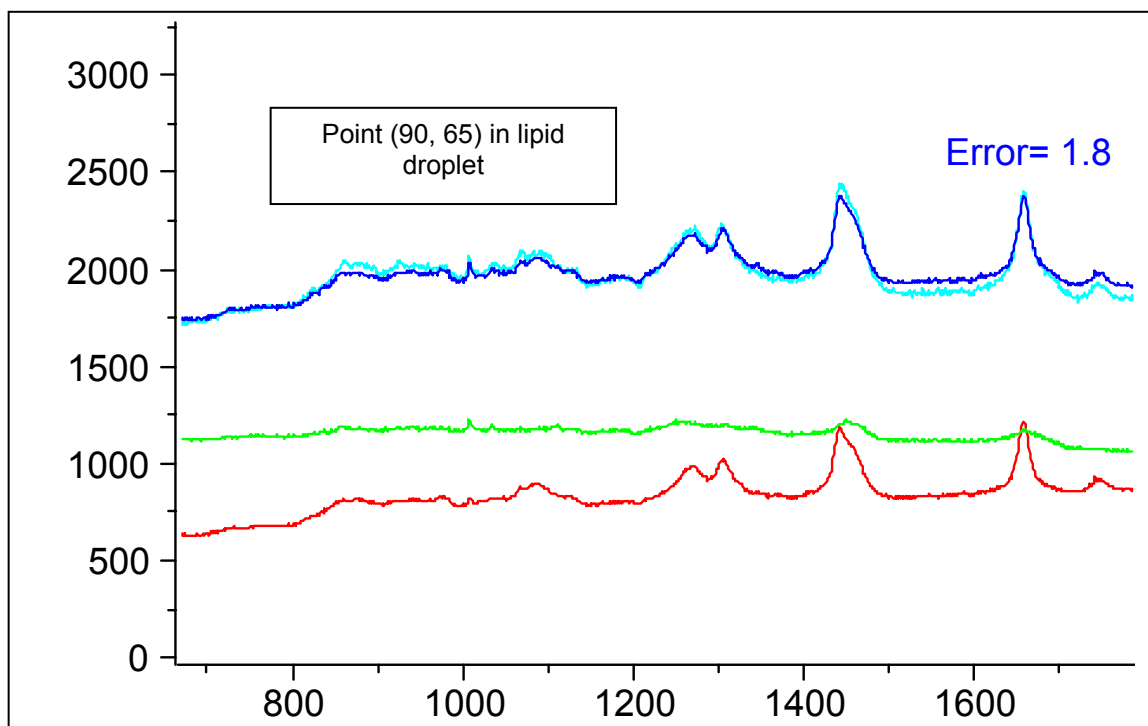


Figure 9. Modelling of spectrum from point in a lipid droplet showing % lipid, % protein, simulated spectrum overlaid on measured spectrum, and % error.

The last figure (10) shows a comparison between fat spectra recorded from a wild-type mouse fed on the Normal Chow (normal fat level) vs. another wild-type mouse fed on the Breeder Chow (high fat level) diet. The big difference between these two spectra is the ratio of the intensities of the  $>C=C<$  ( $1650\text{ cm}^{-1}$ ) to the  $>C=O$  ( $1750\text{ cm}^{-1}$ ) bands. The spectra are displayed so that the intensity of the  $>C=O$  band is about the same in the two spectra. The intensity of the double bond is approximately doubled in the Breeder Chow diet relative to the Normal Chow diet.

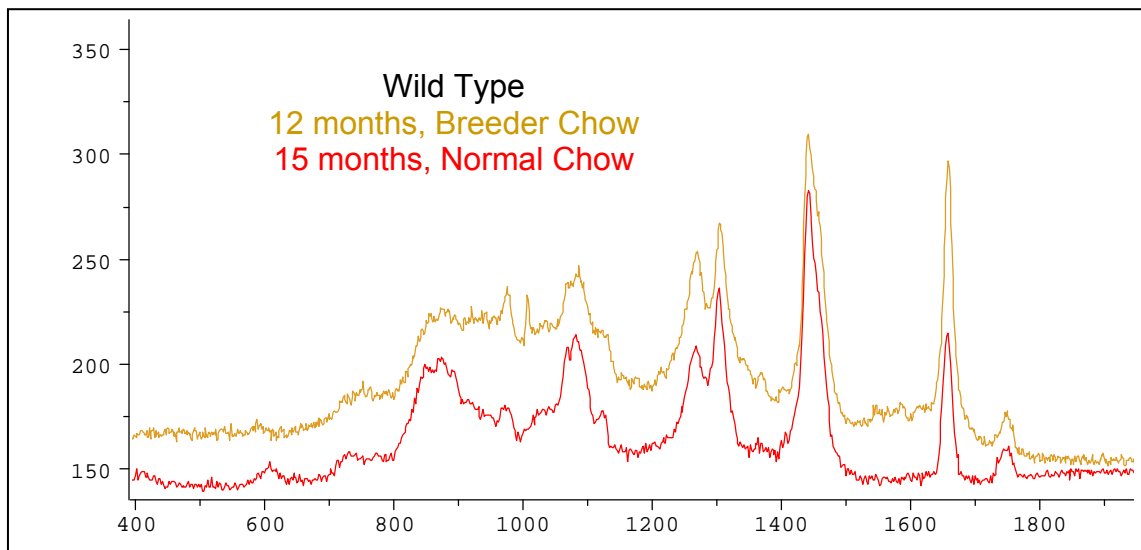


Figure 10. Raman spectrum of fat cells of the wild type mouse fed on Breeder Chow (top) and Normal Chow (bottom).

By referring to Table I showing the fatty acid composition of the two diets it becomes possible to determine how the diet influences the relative intensities of these bands. Note that the monounsaturates contain 1 double bond, linoleic acid contains two double bonds, and linolenic acid contains 3 double bonds, with no conjugation in the doubly and triply unsaturated fatty acids. The relative amounts of double bonds can be calculated, and are shown in Table II.

|                 | %, Normal Chow | %, Breeder Chow | # Double Bonds – Normal Chow | # Double Bonds – Breeder Chow |
|-----------------|----------------|-----------------|------------------------------|-------------------------------|
| Monounsaturates | 1.04           | 3.01            | 1.04                         | 3.01                          |
| Linoleic Acid   | 2.26           | 2.34            | 4.52                         | 4.68                          |
| Linolenic Acid  | 0.20           | 0.26            | 0.60                         | 0.78                          |
| Total           |                |                 | 6.16                         | 8.47                          |

Table II. Fat composition of Normal Chow and Breeder Chow diets, based on % fatty acid type, and # double bonds.

Based on this crude calculation, it would be expected that there is about 1/3 more unsaturation in the Breeder Chow diet than the Normal Chow diet ( $8.47/6.16 = 1.375$ ). The fact that the relative intensity of the double bond in the Raman spectrum increases by a factor of about 2 instead of 1.3 may mean that **unsaturated fatty acids are preferentially being incorporated into the fat cells/globules of the wildtype mouse.**

### 3. Conclusions

FTIR and Raman microprobe spectra were recorded from wild-type (C57BL/6J) and Apo E knock-out mice in order to determine what type of chemical information can be derived from this technique that can complement histopathological observations. In addition to being able to differentiate protein from fatty tissue the following new observations were made.

1. The apo E knock-out mouse showed evidence of globules of free fatty acid not seen in previous studies.
2. A 15 month old mouse (quite old) fed on a normal fat diet showed calcification in the form of calcite possibly due to low levels of the carbonic anhydrase enzyme, or low levels of its activity.
3. Confocal Raman measurements, especially in the form of depth profiles and maps, enable localization of protein and lipid on a scale that increases chemical information that can be correlated with histological studies.
4. Comparison of the lipid spectra from animals fed on normal fat vs. high fat diets shows that it will be possible to measure how much unsaturation is incorporated into the animal.

### References

<sup>1</sup>TJ Romer, et.al., Intravascular ultrasound combined with Raman spectroscopy to localize and quantify cholesterol and calcium salts in atherosclerotic coronary arteries, *Arteriosclerosis, Thrombosis, and Vascular Biology*, 20(2), 478, 2000

<sup>2</sup>ZAFayad, and V Fuster, Clinical imaging of the high-risk or vulnerable atherosclerotic plaque, *Cir. Res.* 89(4), 305-16, 2001

<sup>3</sup>PR Moreno and JE Muller, Identification of high-risk atherosclerotic plaques: a survey of spectroscopic methods, *Curr Opin Cardio.* 17(6), 638-47 (2003)

<sup>4</sup>Buischman, et.al, In vivo determination of the molecular composition of artery wall by intravascular Raman spectroscopy, *Anal Chem.* 72, 3771-3775 (2000)

<sup>5</sup>SW Van de Poll, et.al., Imaging of atherosclerosis. Raman spectroscopy of atherosclerosis, *J*

---

Cardiovasc. Risk 9(5), 255-261 (2002)

<sup>6</sup> SW Van de Poll, et.al., Raman spectroscopic investigation of atorvastatin, amlodipine, and both on atherosclerotic plaque development in APOE\*3 Leiden transgenic mice, *Atherosclerosis* 164(1), 65-71 (2002)

<sup>7</sup> JL Breslow, Mouse models of Atherosclerosis, *Science* 272 (5262), 685-688 (1996)

<sup>8</sup> JA Piedrahita, et.al, Generation of mice carrying a mutant apolipoprotein E gene inactivated by gene targeting in embryonic stem cells, *Proc. Natl. Acad. Sci. USA* 89, 4471-4475 (1992)

<sup>9</sup> SH Zhang, et.al., Diet-induced Atherosclerosis in mice heterozygous and homozygous for apolipoprotein E gene disruption, *J Clin. Invest.* 94(3), 937-945 (1994)